COMMUNICATIONS IN COMPUTATIONAL PHYSICS
Vol. **5**, No. 2-4, pp. 582-599

Commun. Comput. Phys.
February 2009

A Fourier Spectral Moving Mesh Method for the Cahn-Hilliard Equation with Elasticity

W. M. Feng[1], P. Yu[2], S. Y. Hu[3], Z. K. Liu[1], Q. Du[1,2,*] and L. Q. Chen[1]

[1] *Department of Materials Science and Engineering, Pennsylvania State University, University Park, PA 16802, USA.*
[2] *Department of Mathematics, Pennsylvania State University, University Park, PA 16802, USA.*
[3] *Pacific Northwest National Laboratory, Richland, WA 99354, USA.*

Received 24 September 2007; Accepted (in revised version) 27 December 2007

Available online 1 August 2008

Abstract. In recent years, Fourier spectral methods have emerged as competitive numerical methods for large-scale phase field simulations of microstructures in computational materials sciences. To further improve their effectiveness, we recently developed a new adaptive Fourier-spectral semi-implicit method (AFSIM) for solving the phase field equation by combining an adaptive moving mesh method and the semi-implicit Fourier spectral algorithm. In this paper, we present the application of AFSIM to the Cahn-Hilliard equation with inhomogeneous, anisotropic elasticity. Numerical implementations and test examples in both two and three dimensions are considered with a particular illustration using the well-studied example of mis-fitting particles in a solid as they approach to their equilibrium shapes. It is shown that significant savings in memory and computational time is achieved while accurate solutions are preserved.

AMS subject classifications: 65M70, 65M50, 74B20

Key words: Phase field, diffuse interface, moving mesh, adaptive mesh, Fourier-spectral method, adaptive spectral method, Cahn-Hilliard equation, elasticity.

1 Introduction

Phase field method has been extensively applied to modeling microstructure evolution for various materials processes including solidification, solid state phase transformations, grain or phase coarsening, etc. It is an attractive and popular approach since the evolution of different microstructural features can be predicted by means of a single set of equations, and there are no explicit boundary conditions defined at interfaces [2, 10].

*Corresponding author. *Email address:* qdu@math.psu.edu (Q. Du)

However, full three-dimensional computer simulations using the phase field method are still computationally challenging in both memory and computational time.

Much of the earlier phase field simulations employed numerical algorithms such as the explicit Euler finite difference method, which suffered severe limitations on the simulation time step and system size. More advanced numerical algorithms have been proposed recently. Generally, these algorithms are designed to increase the numerical stability and the accuracy. Implicit or semi-implicit methods are typically required to increase the time step and improve the stability [10, 14]. To achieve high accuracy in space, two types of approaches have been utilized. One is to employ a spectral representation of a continuous spatial profile of a field variable whenever applicable, e.g. using a Fourier series for a periodic system, and the other is the adaptive mesh approach in which dense grid points are used in the interfacial regions where the field variables have large gradients. The Fourier spectral method and its semi-implicit implementation have shown to be particularly efficient for systems in which the morphologies and microstructures are dominated by long-range elastic interactions [10, 11, 42].

Fourier-spectral methods are best defined for a fixed uniformly distributed spatial mesh. On the other hand, recent studies on adaptive meshing techniques have led to significant improvement of the computational efficiency of traditional fixed grid methods in many applications, including phase field modeling [6, 16, 26, 32, 39]. Particular examples of adaptivity include the mesh refinement and coarsening as well as mesh movement, and it is clear that adaptive mesh methods are useful for microstructures with a very small interfacial width compared to the domain size. An interesting question to be answered is how the efficiency of spectral methods can also be improved through adaptivity. Naturally, many approaches may be offered for different applications [3, 4, 18, 27, 28].

Recently, a new adaptive Fourier-spectral semi-implicit method (AFSIM) is developed which takes advantages of both the moving mesh method and the Fourier Spectral Semi-implicit scheme [17, 40]. With periodic boundary conditions, the key ingredients making the new adaptive method highly efficient and different from some traditional ones include the utilization of a varying physical domain cell for the Fourier spectral implementation and the coupling of iterative schemes with semi-implicit time discretization. A comparison of different ways to incorporate the moving mesh strategy was given in [40] along with some preliminary discussion on the application of AFSIM to various phase field models. Detailed implementation of AFSIM for the numerical solution of the Allen-Cahn equation has been presented in [17] which has demonstrated that it is possible to keep the high accuracy using AFSIM with larger time steps and fewer grid points than previous algorithms. Many solid state phase transformations and microstructure involve the solution of the Cahn-Hilliard diffusion equation and the elasticity equation. Furthermore, the elastic modulus is not only generally anisotropic, but also inhomogeneous, i.e. its magnitude and anisotropy depend on composition, and thus are spatially dependent. In these cases, the implementation of AFSIM is significantly more challenging.

The work here continues our earlier discussions and represents the first attempt, as

we are aware of, to demonstrate the effectiveness of solving the Cahn-Hilliard diffusion model with inhomogeneous, anisotropic elasticity using a combination of adaptive moving mesh and semi-implicit Fourier spectral method. We consider the specific example of coherent precipitates in a solid matrix as they approach to their equilibrium morphology which play an important role in determining the physical properties of a material. Thermodynamically, the shape of a precipitate is determined by both the interfacial energy and elastic energy while kinetically the evolution of a precipitate is achieved through diffusion. The interfacial energy is dominant in determining the particle shape at small sizes, while the elastic energy becomes more important at larger sizes [23]. Therefore, the application of an adaptive moving mesh method is very appealing for the simulation of these excellent examples of microstructure evolutions in many alloy systems that require the solution of diffusion equations coupled with elasticity.

The paper is organized as follows: in Section 2, a brief description of variational formulation based moving mesh techniques is given along with their implementations in Fourier spectral methods. Applications to Cahn-Hilliard equations and the associated elasticity equations are considered in Section 3. Numerical examples are presented in Section 4 with a final conclusion given in Section 5.

2 Variational formulations of moving mesh PDEs

A number of different approaches have been developed in the literature regarding the mesh adaptivity such as adding and removing grid points, reconnecting grid points and also redistributing grid points. For time dependent problems, the redistribution of mesh points may be dynamically performed, leading to the moving mesh methods. Our present study focuses on the latter category. One advantage of such an approach lies in the preservation of the mesh topology, which are important for numerical approximations based on Fourier pseudo-spectral methods.

2.1 Moving mesh PDEs

Moving-mesh PDEs (MMPDEs) can be formulated either on a computational domain [9] or on a physical domain [20]. Numerical illustrations and comparisons of both approaches have been given in [40] which revealed some interesting behavior in the way grids are redistributed. In this paper, as in [17], we consider mainly the physical domain based variational formulation (PDVF), which is derived on a more rigorous basis, though with a slightly more complicated MMPDE. The criteria for redistributing the mesh are usually expressed as certain variational principles. Their solution via the gradient flow approach leads to the so-called moving mesh partial differential equations [20–22]. There are also other strategies such as those based on a posteriori error analysis. We note that in the gradient flow, time can also be viewed as an artificial relaxation variable.

To be more specific, one can get the high grid density in the high gradient region in the physical domain Ω_p (parameterized by $\boldsymbol{x}$) by smoothing the gradient in the compu-

tational domain Ω_c (parameterized by $\boldsymbol{\xi}$) [17, 40]. For this purpose, a mapping $\boldsymbol{x}(\boldsymbol{\xi})$ is constructed from the computational domain to the physical domain such that the representation $v(\boldsymbol{\xi})=u(\boldsymbol{x}(\boldsymbol{\xi}))$ of the physical solution $u=u(\boldsymbol{x})$ in the computational domain is *better behaved* [5,9,20,25,37,38]. The criteria for constructing the mapping are usually expressed as certain variational principles. For instance, the mesh PDE for $\boldsymbol{x}=\boldsymbol{x}(\boldsymbol{\xi})$ can take on the form like $\nabla_{\boldsymbol{\xi}}\cdot(w\nabla_{\boldsymbol{\xi}}\boldsymbol{x})=0$ with suitable boundary conditions, yielding solutions that minimize the functional

$$\int_{\Omega_c} w|\nabla_{\boldsymbol{\xi}}\boldsymbol{x}|^2 d\Omega_c$$

so that the mesh tends to concentrate near where w is large [37]. Here w is the so called monitor function that connects the mesh with the physical solution u. A particular form of w which is adopted in this paper is given by

$$w=\sqrt{1+\beta^2|\nabla_{\boldsymbol{\xi}}u|^2},$$

where β is a scaling constant for the control of mesh concentration. For additional discussion on the choice of monitor functions and the parameters, we refer to [9,20,38,40].

For the physical domain based PDVF approach [20], the aim is to find the inverse mapping $\boldsymbol{\xi}=\boldsymbol{\xi}(\boldsymbol{x},t)$ of $\boldsymbol{x}=\boldsymbol{x}(\boldsymbol{\xi},t)$. Given an appropriate matrix monitor function G, the mapping $\boldsymbol{\xi}=\boldsymbol{\xi}(\boldsymbol{x},t)$ can be constructed by solving the following variational problem

$$\min_{\boldsymbol{\xi}(\boldsymbol{x})} I(\boldsymbol{\xi})=\int_{\Omega_p}\sum_i(\nabla_x\xi^i)^T G^{-1}\nabla_x\xi^i d\boldsymbol{x}. \tag{2.1}$$

The matrix form of G allows the introduction of anisotropically distributed mesh points. The variational problem (2.1) can be solved via a gradient flow, leading to the moving mesh PDE (MMPDE):

$$\frac{\partial}{\partial t}\xi^i(\boldsymbol{x},t)=p\nabla_x\cdot(G^{-1}\nabla_x\xi^i),\quad i=1,2,3, \tag{2.2}$$

where the mobility p is a positive function and can vary in space.

By interchanging the roles of dependent and independent variables in (2.2), the equation (2.2) may be more conveniently given in the computational domain. Using the covariant and contravariant basis vectors as in [20], $\boldsymbol{a}_i=\partial\boldsymbol{x}/\partial\xi^i$, $\boldsymbol{a}^i=\nabla_x\xi^i$ for $i=1,2,3$, and the Jacobian $J=\boldsymbol{a}_1\cdot(\boldsymbol{a}_2\times\boldsymbol{a}_3)$, the equation (2.2) can be transformed into

$$\frac{\partial\boldsymbol{x}}{\partial t}=p\left[\sum_{i,j}(\boldsymbol{a}^i\cdot G^{-1}\boldsymbol{a}^j)\frac{\partial^2\boldsymbol{x}}{\partial\xi^i\partial\xi^j}-\sum_{i,j}\left(\boldsymbol{a}^i\cdot\frac{\partial G^{-1}}{\partial\xi^j}\boldsymbol{a}^j\right)\frac{\partial\boldsymbol{x}}{\partial\xi^i}\right].$$

In case of Winslow type of monitor function $G=wI$ [37], where w is a scalar and I the identity matrix, the above equation can be further simplified into

$$\frac{\partial\boldsymbol{x}}{\partial t}=\frac{p}{w^2}\sum_{i,j}(\boldsymbol{a}^i\cdot\boldsymbol{a}^j)\frac{\partial}{\partial\xi^i}\left(w\frac{\partial\boldsymbol{x}}{\partial\xi^j}\right). \tag{2.3}$$

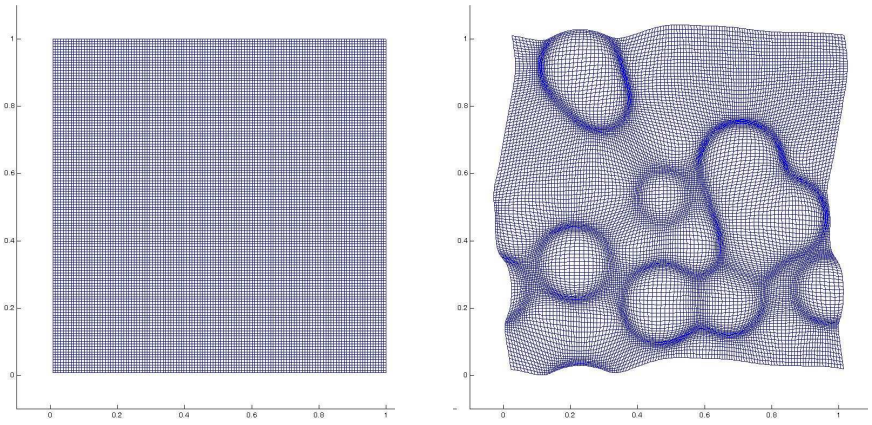

Figure 1: A regular grid on the computational domain (unit square) is mapped to an adaptive grid on the physical domain (non-square).

Discussions on the mobility function p have been made in [17,40], along with a comparison of the equation (2.3) with its counterpart in the computational domain approach. A simpler choice of the mobility function (than that given in [20]) has been proposed as $p=\mu w^2/\lambda$ where λ is the largest eigenvalue of the positive-definite matrix $A=(A_{i,j})=(\boldsymbol{a}^i\cdot\boldsymbol{a}^j)$. The generic constant μ used in p controls the artificial time scale of the MMPDE as compared with the physical time t.

2.2 Fourier-spectral implementation

To match with the periodic boundary condition used in the Fourier-spectral methods for phase field simulations, an important contribution has been made in [17,40] where periodic boundary conditions are adopted for the MMPDE thus allowing a changing physical domain cell. Given a computational domain on a unit square $[0,1]\times[0,1]$, the displacement of the adaptive grid point from its inverse image on the regular grid, i.e. $\boldsymbol{X}(\boldsymbol{\xi},t)=\boldsymbol{x}(\boldsymbol{\xi},t)-\boldsymbol{\xi}$, satisfies the periodic boundary conditions on the unit square, that is,

$$\boldsymbol{x}(\boldsymbol{\xi}+(k,l),t)=\boldsymbol{x}(\boldsymbol{\xi},t)+(k,l),\qquad \forall \text{ integer pair } (k,l)\,. \tag{2.4}$$

Interestingly, this condition does not require that $\boldsymbol{x}(\boldsymbol{\xi},t)$ maps a unit square onto a unit square. This observation has also been made in [12] for moving mesh finite element methods for the Navier-Stokes equations. The Fourier spectral implementation considered here allows the mesh moving equations be solved in the similar fashion as the phase field equations. With periodic boundary conditions, the physical domain does not maintain a square shape, while the computational domain does. An illustration is given in Fig. 1 to show how the mesh is adapted to a particular microstructure pattern in the physical domain. Although the physical domain boundaries are curvy, the condition (2.4) guarantees that the periodic copies of Ω_p (a non-square shape) cover the whole 2-dimensional space as effectively as periodic copies of the unit square. In particular, it can

be seen that (2.4) implies that the area of the physical domain Ω_p is the same as that of Ω_c.

For the physical domain PDVF approach studied here, in terms of $\boldsymbol{X}$, (2.3) becomes

$$\frac{\partial \boldsymbol{X}}{\partial t}=\mu\sum_{i,j}\frac{\boldsymbol{a}^i\cdot\boldsymbol{a}^j}{\lambda}\frac{\partial}{\partial\xi^i}\left[w(\frac{\partial \boldsymbol{X}}{\partial\xi^j}+e^j)\right], \tag{2.5}$$

where e^i is the canonical unit vector (ith column of the identity matrix). The semi-implicit Fourier spectral (or Fourier collocation, Fourier pseudo-spectral) scheme can be used to solve it numerically. A particular form as used in [17], in the Fourier variables, is given by

$$(1+\mu W\delta\tau\boldsymbol{k}^2)(\hat{\bar{\boldsymbol{X}}}-\hat{\boldsymbol{X}})=\mu\delta\tau\left\{\sum_{i,j}\frac{\boldsymbol{a}^i\cdot\boldsymbol{a}^j}{\lambda}\frac{\partial}{\partial\xi^i}\left[w(\frac{\partial \boldsymbol{X}}{\partial\xi^j}+e^j)\right]\right\}^{\wedge}, \tag{2.6}$$

where $\bar{\boldsymbol{X}}$ is the value of $\boldsymbol{X}$ at the next time step, W is the maximum of w on Ω_c, $\boldsymbol{k}$ denotes the wave vector, and $\wedge$ represents the Fourier transform.

3 Cahn-Hilliard equation

The Cahn-Hilliard equation with constant mobility and elasticity is

$$\frac{\partial}{\partial t}c(\boldsymbol{x},t)=\triangle_{\boldsymbol{x}}\frac{\delta F}{\delta c}=\triangle_{\boldsymbol{x}}(\frac{\partial}{\partial c}f(c)+\frac{\partial}{\partial c}e-\epsilon^2\triangle_{\boldsymbol{x}}c), \tag{3.1}$$

where c is the composition, F the total free energy, f the local free energy, e the elastic energy, and ϵ the gradient energy coefficient. Microstructure evolution takes place to reduce the total free energy in the system that may include the bulk chemical free energy, interfacial energy, and the long-range interaction energies such as the elastic energy.

In recent years, phase field models have been developed to incorporate the elastic effect by expressing the elastic strain energy as a function of field variables (see for example, [19, 42] and the references cited therein). To be specific, the elastic energy density in the Cahn-Hilliard equation Eq. (3.1) can be calculated by $e=\frac{1}{2}C_{ijkl}\varepsilon^{el}_{ij}\varepsilon^{el}_{kl}$ with a summation convention. Here the elastic strain ε^{el} is the difference between total strain ε and stress-free strain ε^0 since stress-free strain does not contribute to the total elastic energy, i.e. $\varepsilon^{el}_{kl}=\varepsilon_{kl}-\varepsilon^0_{kl}$, while $\varepsilon_{kl}=\bar{\varepsilon}_{kl}+\delta\varepsilon_{kl}$ with $\bar{\varepsilon}$ being the homogeneous strain which determines the macroscopic shape and volume change produced by internal stress and externally applied stress, $\delta\varepsilon$ the inhomogeneous local strain which is related to the local displacement field u by the usual elasticity relation,

$$\delta\varepsilon_{kl}=\frac{1}{2}\left(\frac{\partial u_k}{\partial x_l}+\frac{\partial u_l}{\partial x_k}\right).$$

We now discuss the application of adaptive Fourier spectral semi-implicit scheme for the Cahn-Hilliard equation coupled with the elasticity equation.

3.1 Moving mesh formulation of the Cahn-Hilliard equation

Treating c as a function of $\boldsymbol{\xi}$ and t, we have

$$\frac{\partial}{\partial t}c(\boldsymbol{\xi},t)=\dot{\boldsymbol{x}}\cdot\nabla_{\boldsymbol{x}}c+\triangle_{\boldsymbol{x}}(\frac{\partial}{\partial c}f(c)+\frac{\partial}{\partial c}e-\epsilon^2\triangle_{\boldsymbol{x}}c), \tag{3.2}$$

where $\dot{\boldsymbol{x}}=\partial\boldsymbol{x}(\boldsymbol{\xi},t)/\partial t$ is the mesh velocity determined from the MMPDEs. The convection term $\dot{\boldsymbol{x}}\cdot\nabla_{\boldsymbol{x}}c$ represents the change of the inverse image of the field variable c on the computational domain due to the mesh motion. Using the notation defined earlier, one may easily verify

$$\nabla_{\boldsymbol{x}}c=\sum_i \boldsymbol{a}^i\frac{\partial c}{\partial\xi^i},\quad \triangle_{\boldsymbol{x}}c=\frac{1}{J}\nabla_{\boldsymbol{\xi}}\cdot(JA\nabla_{\boldsymbol{\xi}}c),$$

where $A=(A_{i,j})=(\boldsymbol{a}^i\cdot\boldsymbol{a}^j)$. In order to apply the semi-implicit Fourier spectral scheme, we denote by λ^* the maximum among the eigenvalues of A over Ω_c, and introduce the splitting in the Fourier space:

$$(1+(\lambda^*\boldsymbol{k}^2)^2\delta t)(\hat{\bar{c}}-\hat{c})=\delta t\left\{\dot{\boldsymbol{x}}\cdot\nabla_{\boldsymbol{x}}c+\triangle_{\boldsymbol{x}}(\frac{\partial}{\partial c}f(c)+\frac{\partial}{\partial c}e-\epsilon^2\triangle_{\boldsymbol{x}}c)\right\}^{\wedge}. \tag{3.3}$$

We may also split the nonlinear term to get a modified scheme

$$(1+(\lambda^*\boldsymbol{k}^2)^2\delta t+\sigma^*\boldsymbol{k}^2\delta t)(\hat{\bar{c}}-\hat{c})=\delta t\left\{\dot{\boldsymbol{x}}\cdot\nabla_{\boldsymbol{x}}c+\triangle_{\boldsymbol{x}}(\frac{\partial}{\partial c}f(c)+\frac{\partial}{\partial c}e-\epsilon^2\triangle_{\boldsymbol{x}}c)\right\}^{\wedge}, \tag{3.4}$$

where $\sigma^*>0$ is chosen such that $f(c)+\sigma^*c$ remains monotone for physically meaningful values of c. The addition of terms involving λ^* and σ^* effectively introduces damping terms like $\delta t(\lambda^*\triangle_{\boldsymbol{x}})^2$ and $-\delta t\sigma^*\triangle_{\boldsymbol{x}}$ to the left hand side of the equation (3.2). The splitting reduces the stiffness of the equation, helps maintaining the stability, and allows the efficient implementation using FFT.

3.2 Inhomogeneous elasticity equations and an iterative scheme

We first recall the treatment of the homogeneous elasticity system corresponding to the following mechanical equilibrium equation:

$$\lambda_{ijkl}\frac{\partial^2}{\partial x_j\partial x_l}u_k^0=\lambda_{ijkl}\frac{\partial\delta c}{\partial x_j}\varepsilon_{kl}^0, \tag{3.5}$$

where $\delta c=c(\boldsymbol{x})-c_0$, λ_{ijkl} the homogeneous elasticity modulus tensor, u^0 the local displacement in the homogeneous (zeroth order) approximation, ε^0 the local stress-free strain, and c_0 the average composition as the zero stress reference.

Under the variable transform $\boldsymbol{\xi}\to\boldsymbol{x}$, the elasticity system can be rewritten as

$$\lambda_{i\alpha k\beta}\frac{\partial\xi_j}{\partial x_\alpha}\frac{\partial}{\partial\xi_j}\left(\frac{\partial\xi_l}{\partial x_\beta}\frac{\partial u_k^0}{\partial\xi_l}\right)=\lambda_{ijkl}\frac{\partial\delta c}{\partial x_j}\varepsilon_{kl}^0. \tag{3.6}$$

We first introduce a splitting to majorize the 4-rank tensor

$$\tilde{\lambda}_{ijkl}=\lambda_{i\alpha k\beta}\frac{\partial\boldsymbol{\xi}_j}{\partial x_\alpha}\frac{\partial\boldsymbol{\xi}_l}{\partial\boldsymbol{x}_\beta}.$$

In particular, we want to control $\tilde{\lambda}_{ijkl}$ by a scalar ν^2 multiple of λ_{ijkl} in the sense that for any matrix (p_{ij}),

$$\nu^2 p_{ij}\lambda_{ijkl}p_{kl}\geq p_{ij}\tilde{\lambda}_{ijkl}p_{kl}\,.$$

The constant ν is chosen to be the Frobenius norm of $\partial\xi_i/\partial x_j$, i.e.,

$$\nu^2=\sum_i\sum_j\left(\frac{\partial\xi_i}{\partial x_j}\right)^2.$$

After the splitting, we have the equivalent representation of the elasticity system,

$$\nu^2\lambda_{ijkl}\frac{\partial^2u_k^0}{\partial\xi_j\partial\xi_l}+\lambda_{ijkl}\frac{\partial^2u_k^0}{\partial x_j\partial x_l}=\lambda_{ijkl}\frac{\partial\delta c}{\partial x_j}\varepsilon_{kl}^0+\nu^2\lambda_{ijkl}\frac{\partial^2u_k^0}{\partial\xi_j\partial\xi_l} \tag{3.7}$$

and arrive at the iterative-perturbation scheme as in [42],

$$\nu^2\lambda_{ijkl}\frac{\partial^2(\tilde{u}_k^0-u_k^0)}{\partial\xi_j\partial\xi_l}=\lambda_{ijkl}\frac{\partial\delta c}{\partial x_j}\varepsilon_{kl}^0-\lambda_{ijkl}\frac{\partial^2u_k^0}{\partial x_j\partial x_l},$$

where $\tilde{u}_k^0$ is the new value of u_k^0 after the iteration. We can also view the scaling factor ν as an effective time scale introduced for the iterative scheme.

The above iterative scheme in the Fourier spectral setting is given by

$$\hat{\tilde{u}}_k^0=\hat{u}_k^0-\frac{\Omega_{ij}}{\kappa^2\nu^2}\left(\lambda_{ijkl}\frac{\partial\delta c}{\partial x_j}\varepsilon_{kl}^0-\lambda_{ijkl}\frac{\partial^2u_k^0}{\partial x_j\partial x_l}\right)^\wedge, \tag{3.8}$$

where $\Omega_{ij}^{-1}=\lambda_{ijkl}n_kn_l$, κ being the magnitude of the wave vector, and n the normalized wave vector. For an inhomogeneous elasticity system

$$\frac{\partial}{\partial x_j}\left(C_{ijkl}\frac{\partial u_k}{\partial x_l}\right)=\frac{\partial\delta c}{\partial x_j}\left[(2\lambda'_{ijkl}\delta c+\lambda_{ijkl})\varepsilon_{kl}^0-\lambda'_{ijkl}\bar{\varepsilon}_{kl}\right], \tag{3.9}$$

where $C_{ijkl}=\lambda_{ijkl}+\lambda'_{ijkl}\delta c$ is the elasticity modulus with a homogeneous part λ_{ijkl} and an inhomogeneous part $\lambda'_{ijkl}\delta c$ [19], similar to the homogeneous case, we introduce the variable transform $\boldsymbol{\xi}\to\boldsymbol{x}$ and the splitting scheme. After the splitting, we have the equivalent representation of the elasticity system:

$$\nu^2\lambda_{ijkl}\frac{\partial^2\tilde{u}_k}{\partial\xi_j\partial\xi_l}+\frac{\partial}{\partial x_j}\left(C_{ijkl}\frac{\partial u_k}{\partial x_l}\right)=\frac{\partial\delta c}{\partial x_j}\left[(2\lambda'_{ijkl}\delta c+\lambda_{ijkl})\varepsilon_{kl}^0-\lambda'_{ijkl}\bar{\varepsilon}_{kl}\right]+\nu^2\lambda_{ijkl}\frac{\partial^2u_k}{\partial\xi_j\partial\xi_l}$$

and arrive at analog of the iterative-perturbation scheme as in [42],

$$\lambda_{ijkl}\frac{\partial^2(\tilde{u}_k-u_k)}{\partial\xi_j\partial\xi_l}=\frac{1}{\nu^2}\left\{\frac{\partial\delta c}{\partial x_j}\left[(2\lambda'_{ijkl}\delta c+\lambda_{ijkl})\varepsilon^0_{kl}-\lambda'_{ijkl}\bar{\varepsilon}_{kl}\right]-\frac{\partial}{\partial x_j}\left(C_{ijkl}\frac{\partial u_k}{\partial x_l}\right)\right\}, \tag{3.10}$$

where $\tilde{u}_k$ is the new value of u_k after the iteration. Simplifying and formulating in the Fourier space, we obtain the final form of the iterative-perturbation scheme

$$\hat{\tilde{u}}_k=\hat{u}_k-\frac{\Omega_{ij}}{\kappa^2\nu^2}\left\{\frac{\partial\delta c}{\partial x_j}\left[(2\lambda'_{ijkl}\delta c+\lambda_{ijkl})\varepsilon^0_{kl}-\lambda'_{ijkl}\bar{\varepsilon}_{kl}\right]-\frac{\partial}{\partial x_j}\left(C_{ijkl}\frac{\partial u_k}{\partial x_l}\right)\right\}^{\wedge}. \tag{3.11}$$

We refer to [40] for more discussions on the computational cost.

3.3 Switching on the mesh adaptation

The adaptive Fourier spectral methods bring potentially significant savings, but they are also associated with extra overhead costs. The savings become more dramatic when the interfacial regions are more concentrated spatially. In practice, the mesh adaption can be used as an independent module to complement the existing phase field simulation on a uniform mesh, and mesh adaptation can be switched on only when the potential payoff is evident. There are two important factors that affect this decision: efficiency and accuracy.

More specifically, we are concerned with whether the computational savings resulting from the mesh adaptation would out-weigh the overheads caused by the extra Fourier transforms required to solve the phase field equations in the computational domain. Meanwhile, as much as we would like to save on a smaller (adaptive) grid, we cannot sacrifice the computational accuracy. Following the discussions given in [40], in practice, we may take the guideline that the mesh adaption will be switched on when the volume fraction of the interfacial region falls below certain threshold chosen for the particular simulation, and lock in the savings by successively reducing the grid size provided that it still allows accurate determination of the driving forces. Since the solution behavior away from the interfacial region also affects the interface motion, we anticipate that a better alternative than this heuristic rule may be developed based on a more complete *a posteriori* error analysis.

4 Numerical simulations and discussion

We now present numerical examples to illustrate the effectiveness of the adaptive Fourier-spectral Semi-implicit method (AFSIM) for the Cahn-Hilliard equation with elasticity.

4.1 One-dimensional implementation

The first example presented in this paper is to test the accuracy of the proposed adaptive Fourier-spectral Semi-implicit method (AFSIM). We choose the evolution of a cosine

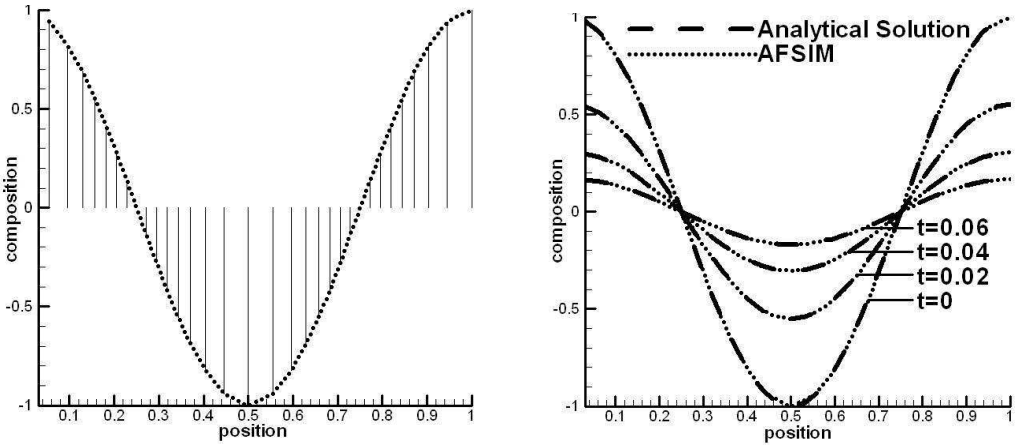

Figure 2: Concentration and mesh distribution of AFSIM (left) and the composition evolution with time (right).

profile $c = c_0(t)\cos(2\pi x)$ with free energy $f(c) = c^2/2$. We consider the Cahn-Hilliard Eq. (3.1) in one dimension without elasticity, so that we have

$$\frac{\partial}{\partial t}c(\boldsymbol{x},t) = \triangle_{\boldsymbol{x}}(c - \epsilon^2 \triangle_{\boldsymbol{x}} c) = -(4\pi^2 + 16\pi^4\epsilon^2)c_0(t)\cos(2\pi x), \tag{4.1}$$

with an exact solution

$$c = e^{-(4\pi^2+16\pi^4\epsilon^2)t}\cos(2\pi x).$$

In the implementation of AFSIM, the system or domain size is taken to be of unit length. We take 32 grid points and $\beta^2 = 0.01$ in the monitor function. This particular value of β is selected without any special consideration but it is found to be a good choice of making the simulation stable. At $t = 0$, an initial composition distribution is prescribed. A certain number of steps (e.g. 100 steps) are performed to prepare for the initial adaptive mesh distribution.

More specifically, during the initial preparation, only MMPDE (2.6) is solved. The change of composition due to the mesh motion $\dot{\boldsymbol{x}} \cdot \nabla_{\boldsymbol{x}} c$ can then be calculated. The composition distribution for the system is updated. After a number of time steps, we get an adaptive mesh distribution (Fig. 2, left). We see that mesh density is higher when composition gradient is higher. After that, the evolution of composition is turned on.

The time step size of mesh motion, denoted by $\delta\tau$ can be different from the time step size δt for the Cahn-Hilliard equation (3.3). In the present simulation, $\delta\tau = 1E-03$ and $\delta t = 1E-05$. The number of mesh motion steps can be performed differently from that for the solution of the PDE. In this simulation, we evolve the mesh and solve the PDE with the same steps once beyond the initial preparation. Once beyond the initial stage, in every time step, the MMPDE is solved first, and the change of composition due to the mesh motion $\dot{\boldsymbol{x}} \cdot \nabla_{\boldsymbol{x}} c$ can then be calculated, followed by the update of the composition distribution for the system using Eq. (3.3). Since an analytical solution for the temporal

evolution kinetics is known, we can compare the simulation results with the analytical solution. Fig. 2 (right) shows the evolution of the composition. Dashed lines are from the analytical solution, dotted lines from simulation. The largest relative L^2 error of the AFSIM solution at any time is about 0.08%. We can thus see that the simulation results agree quite well with the analytical solution. We note that this example is only used to verify the accuracy of the AFSIM. Since the analytic solution does not have spatially highly concentrated derivative, methods based on the uniform mesh can also be very accurate in this case.

4.2 Two-dimensional implementation

We present two examples here. The first example is chosen for testing the accuracy and efficiency of the proposed AFSIM. In light of the numerical studies already carried out in [11] which demonstrated the high efficiency and accuracy of uniform Fourier-spectral semi-implicit method (UFSIM) in comparison with low order methods developed earlier in the literature, we elect to compare the performance of AFSIM and UFSIM. The second example illustrates the effectiveness of the AFSIM in simulating the evolution of random microstructure.

To compare the accuracy and efficiency of various schemes, we first consider the Cahn-Hilliard Eq. (3.1) with inhomogeneous elasticity in two dimensions (again with unit system or domain size) with various grid sizes dx and time step sizes δt and $\delta\tau$ (note a grid size of $dx=1/64$ implies the number of grid points used is 64×64). The double-well free energy $f(c)=-c^2/2+c^4/4$ is used in this case. The other parameters are chosen without any special consideration. For example, the gradient coefficient is chosen to be $\epsilon=0.002$, ε^0_{ij} is assumed purely dilatational $\varepsilon^0_{ij}=0.04\delta_{ij}$ with I being the identity matrix, and $\lambda_{11}=600$, $\lambda_{12}=400$, $\lambda_{44}=200$, $\lambda'_{11}=-100$, $\lambda'_{12}=-75$, $\lambda'_{44}=-25$.

At $t=0$, a circular domain with a radius of 0.25 is prescribed. The composition values are assigned $+1$ inside the circle and -1 outside using

$$c=-\tanh((\sqrt{(x-0.5)^2+(y-0.5)^2}-0.25)/\epsilon).$$

The interface is automatically generated by the tanh function. We first take 500 steps of the MMPDE to generate the initial mesh, same as in the above example. After that, in each step, Eq. (2.6) is first solved to evolve the mesh. The elasticity equation (3.8) is then solved for an elastically homogeneous modulus system, and the iterative procedure (Eq. (3.11)) is used to obtain the elasticity solution for the more general, inhomogeneous modulus case. With the equilibrium elastic displacements, the composition distribution for the system is updated using Eq. (3.3).

The evolution of the circular domain from phase field simulations is shown in Figs. 3 and 4 for an elastically inhomogeneous cubic system with anisotropy parameter

$$\psi=2\lambda_{44}/(\lambda_{11}-\lambda_{12})>1.$$

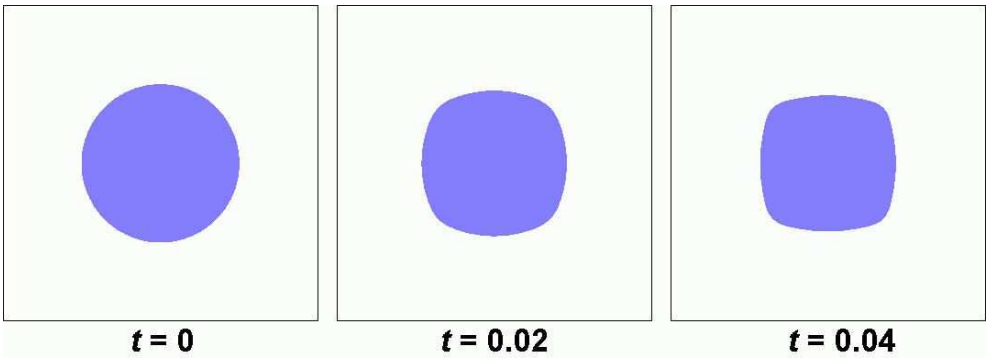

Figure 3: Concentration distribution for the 2d circular domain simulation.

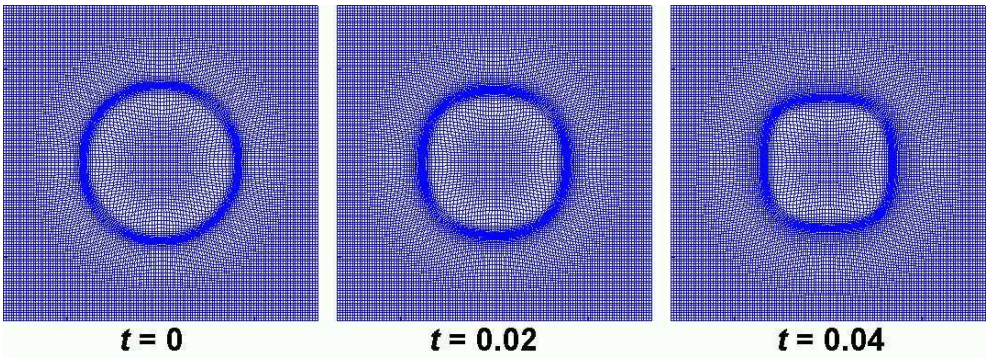

Figure 4: Mesh distribution for the 2d circular domain simulation.

As previously predicted by others, the precipitate shape gradually changes from a sphere to a cube with the sides along the $\{100\}$ planes. So the moving mesh correctly predicts the diffuse-controlled evolution of a coherent precipitate. In the implementation of AFSIM, we take $\beta^2=0.02$ in the monitor function and pick $\mu=1$ to get the mobility in the Eq. (2.6). These are the only extra parameters required in the computer simulation other than those already used in the standard UFSIM.

Since there is no analytical solution for this case, we take the simulation result of UFSIM (with $dx=1/1024$) as the accurate solution. We may characterize the accuracy of different schemes by comparing the final area of the domain with the accurate solution. The resulting relative errors (in terms of the percentage of the area) are shown in Table 1. It is noticeable that with different grid sizes dx and time step sizes δt and $\delta\tau$, the newly developed AFSIM is much more accurate and stable.

The overall computational capacity and computing time are crucial issues in large-scale simulations, especially three-dimensional simulations. AFSIM can significantly increase the spatial scale of the simulation and improve the efficiency, and ensure the computation accuracy as well. Table 2 shows the computing time of both schemes with different grid sizes and time step sizes. One may notice that, by providing a similar accuracy,

Table 1: The error percentages of the area for 2D circular domain.

δt	5E-06	1E-05	5E-05	1E-04
UFSIM $dx=1/256$	0.76	unstable	unstable	unstable
UFSIM $dx=1/128$	1.35	unstable	unstable	unstable
AFSIM $dx=1/64$	0.78	0.79	0.81	0.98

Table 2: The computing time for the 2D circular domain (unit: s).

δt	5E-06	1E-05	5E-05	1E-04
UFSIM $dx=1/256$	5092	–	–	–
UFSIM $dx=1/128$	1124	–	–	–
AFSIM $dx=1/64$	1543	788	157	80

the AFSIM is more than 20 times faster than the UFSIM, in addition to potential memory savings by using fewer grid points.

The AFSIM scheme presented here can be used to simulate more realistic microstructures, although it is expected to perform much better for microstructures with a small fraction of interfaces. We next consider the evolution of a random domain structure. The same free energy and parameters used above are employed unless otherwise specified. $\lambda'_{11}=300$, $\lambda'_{12}=200$, $\lambda'_{44}=100$ and $\epsilon=0.004$. At $t=0$, the initial distribution of phase field parameter is around 0 with a spatial small random noise valued within $(-0.25,0.25)$.

The random structures shown in the left column of Fig. 5 are obtained during the time evolution using UFSIM with $dx=1/256$, $\delta t=5\times10^{-6}$. To compare, we take the distribution at $t=1.2$ using UFSIM as the input for AFSIM. The second column of Fig. 5 shows the mesh distribution during evolution using AFSIM with $dx=1/128$, $\delta t=5\times10^{-5}$, and $\beta^2=0.05$. The associated composition distribution is plotted in the third column of Fig. 5. It can be seen that the results in the different columns of Fig. 5 agree quite well. In the right column of Fig .5 shows the composition distribution from $t=1.20$ to $t=1.30$ using UFSIM with $dx=1/128$ and $\delta t=5\times10^{-6}$. Notice that the microstructure evolution displayed in the right column of Fig .5 is nearly stopped, as seen most evidently in the smallest particle (highlighted in circles), due to insufficient grid points in the interfaces. Thus, the UFSIM with the same degree of freedom as the AFSIM produces qualitatively different results and is unable to accurately reproduce the same morphology as shown in the AFSIM and the finer UFSIM calculation. This again illustrates the enhanced resolution provided by AFSIM over the UFSIM when the same number of grid points is used. Although the accuracy of these two methods cannot be compared quantitatively for the present case because there is no analytical solution, the efficiency of the two methods are studied by using the AFSIM solution with $dx=1/128$ and $\delta t=5\times10^{-5}$ as the benchmark to compare the computational cost involved. It is found that the AFSIM with less Fourier modes and larger time step is five times more efficient than UFSIM with more Fourier modes and smaller time step.

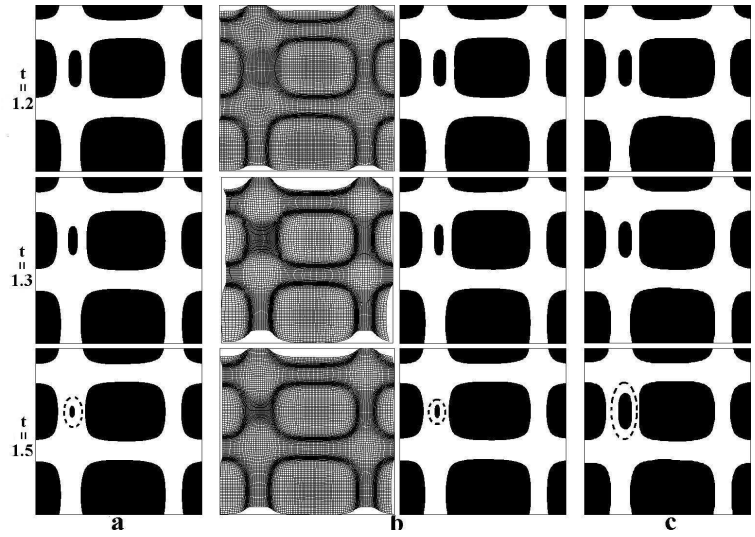

Figure 5: Temporal evolution of a random domain structure: two UFSIM simulations (left and right columns) and an AFSIM simulation along with the moving mesh (two center columns).

4.3 Three dimensional implementation

Recently we have produced the first three dimensional simulation that combined the moving mesh strategy with the Fourier spectral discretization in the context of Allen-Cahn dynamics [17]. Here we use the three-dimensional implementation of AFSIM scheme to examine the equilibrium shapes of the second-phase precipitates. In the following, we consider the Cahn-Hillard Eq. (3.1) with elasticity in three dimensions with a unit system size, and $dx = 1/64$. The other parameters are the same as the second example unless stated otherwise. We first examine the equilibrium shape of a precipitate for a previously studied elastically homogeneous cubic system with negative anisotropy $\psi > 1$ ($\lambda_{11} = 300$, $\lambda_{12} = 175$, $\lambda_{44} = 125$). The equilibrium shapes of the precipitate from phase field simulations are shown in Fig. 6. Same as in the 2D case, the precipitate shape gradually changes from a sphere to a cube with the sides along the $\{100\}$ planes. The equilibrium shapes of the precipitate for the cubic system with positive anisotropy $\psi < 1$ ($\lambda_{11} = 250$, $\lambda_{12} = 100$, $\lambda_{44} = 25$) are also shown in Fig. 7. The shape changes to an octahedron with sides along $\{111\}$ planes. These results agree very well with the previous studies [29, 33].

We note that the simulation using UFSIM with the same parameters is unstable, which gives another demonstration of the advantage of AFSIM.

4.4 Discussions

Because the monitor function automatically gathers mesh points around the interface region and scales mesh appropriately in the computational domain, the stiffness of the solution is reduced. The new method results in significant efficiency savings over uniform

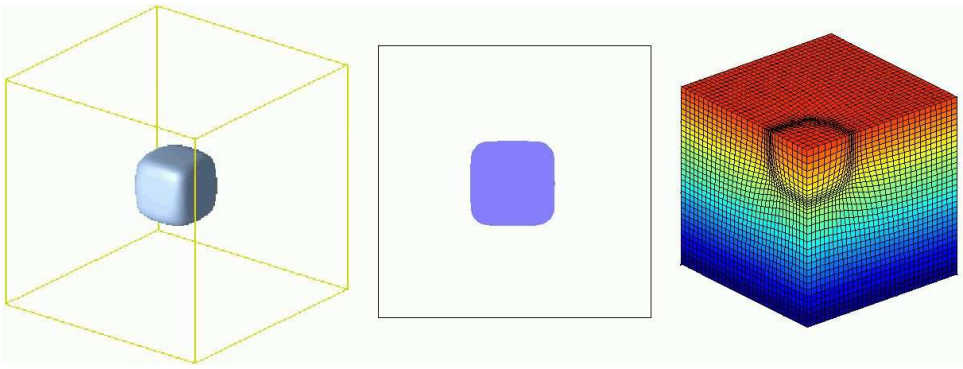

Figure 6: The equilibrium shape, its center section, and the quadrant section of mesh distribution for $\psi>1$.

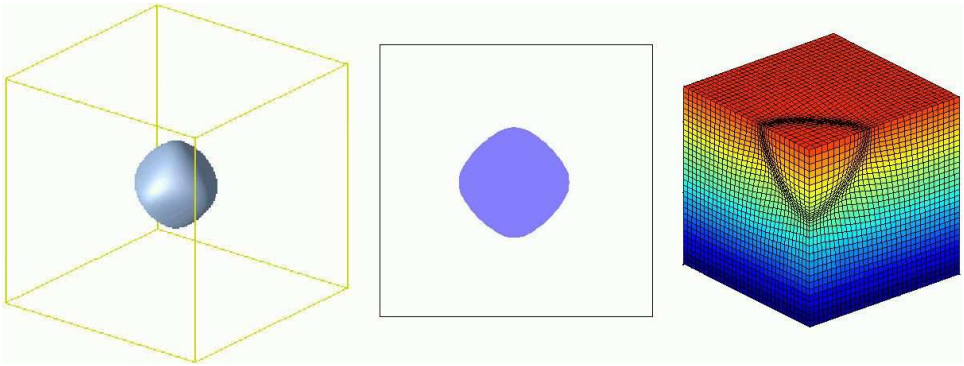

Figure 7: The equilibrium shape, its center section, and the quadrant section of mesh distribution for $\psi<1$.

mesh methods in particular cases. In addition to the savings of Fourier-spectral semi-implicit method, larger time steps and larger grid size can be used without sacrificing the accuracy by taking advantages of the moving mesh method. It should be noticed that the new AFSIM requires more CPU time in constructing a time-dependent mapping from the computational domain to the physical domain, which constitutes the overhead of the moving mesh strategy. Counting the cost of solving MMPDE and Cahn-Hilliard equation with inhomogeneous elasticity together, we need 214 Fourier transforms in 3D. In contrast, solving the Cahn-Hilliard equation with inhomogeneous on a regular uniform grid requires 35 Fourier transforms. Therefore, an adaptive grid with a compression ratio of three in each dimension would already noticeably reduce the overall computational cost. As the number of Fourier modes is reduced, we also see potential savings in the memory. Although the new moving mesh strategy can be used for all problems, the computational efficiency does not improve significantly if the microstructure has high interface volume fraction. In such a case, the mesh distribution tends to be homogeneous, the moving mesh method would lose much of its advantage.

5 Conclusions

A new numerical scheme has been developed to solve the phase field equations. It combines the adaptive moving mesh method with the semi-implicit Fourier spectral algorithm. The scheme has been implemented in both two and three dimensions for solving Cahn-Hilliard equation with elasticity. It is demonstrated that for a prescribed accuracy, the new moving mesh method can potentially lead to an order of magnitude improvement in efficiency over the conventional uniform mesh spectral method. In particular, many alloy systems, e.g. Al alloys, contain a low volume fraction of precipitates with separation distances significantly larger than their dimensions. In such systems, the application of an adaptive moving mesh can be very appealing as the amount of interfaces per unit volume is relatively small. Applications to phase field simulations of microstructure evolution and other processes [10,15,35,43] will be studied in the future. In addition, the examples shown here and those in [17] indicate that with the reduction of the number of Fourier modes, larger time steps can also be taken in the phase field simulation. Intuitively, the adaptive mesh tends to provide better resolution to the large gradients in the solution in both one and higher space dimensions, and in the latter case, the grid distribution is effectively adjusted in an anisotropical fashion. These may all be factors contributing to better time accuracy and stability. It will be interesting to examine such an effect more closely and to investigate the coupling of spatial adaptivity of Fourier spectral methods with the time adaptivity of variable step size.

Acknowledgments

This work has been supported by the National Science Foundation Information Technology Research Project (NSF-ITR) through Grant DMR-0205232. The work of Qiang Du is also supported by NSF-DMS 0712744. The authors would like to thank the referees for their helpful comments and for bringing additional references on the subject to our attention.

References

[1] S.M Allen and J.W. Cahn, A microscopic theory for antiphase boundary motion and its application to antiphase domain coarsening, *Acta Metall. Mater.*, 27 (1979), pp.1085-1095.
[2] D. M. Anderson, G. B. McFadden, and A. A. Wheeler, Diffuse-interface methods in fluid mechanics, *Ann. Rev. Fluid Mech.*, 30 (1998), pp.139–165.
[3] A. Bayliss, D.Gottlieb, B. J. Matkowsky and M. Minkoff, An adaptive pseudo-spectral method for reaction-diffusion problems, *J. Comput. Phys.*, 90 (1998), pp.421-443.
[4] A. Bayliss, R. Kuske and B. J. Matkowsky, A two-dimensional adaptive pseudo-spectral method, *J. Comput. Phys.*, 91 (1990), pp.174-196.
[5] P. Bochev, G. Liao , G. dela Pena, Analysis and computation of adaptive moving grids by deformation, *Numer. Meth. Part. Diff. Eq.*, 12 (1998), pp.489-506.

[6] R. J. Braun and B. T. Murray, Adaptive phase-field computations of dendritic crystal growth, *J. Crystal Growth*, 174 (1997), pp.41-53.
[7] J.W. Cahn and J.E. Hilliard, Free energy of a nonuniform system. I. Interfacial free energy, *J. Chem. Phys.*, 31 (1959), pp.258–267.
[8] W. Cao, W. Huang and R. D. Russell, A Study of Monitor Functions for Two Dimensional Adaptive Mesh Generation, *SIAM J. Sci. Comput.*, 20 (1999), pp.1978-1994.
[9] H. Ceniceros and T. Y. Hou, An Efficient Dynamically Adaptive Mesh for Potentially Singular Problems, *J. Comput. Phys.*, 172 (2001), pp.609-639.
[10] L.Q. Chen, Phase-field models for microstructure evolution, *Ann. Rev. Mater. Sci.*, 32 (2002), pp.113–140.
[11] L.Q. Chen and J. Shen, Applications of semi-implicit Fourier-spectral method to phase field equations, *Comput. Phys. Commun.*, 108 (1998), pp.147-158.
[12] Y. Di, R. Li, T. Tang and P.-W. Zhang, Moving mesh finite element methods for the incompressible Navier-Stokes equations, *SIAM J. Sci. Comput.*, 26 (2005), pp.1036-1056.
[13] E.A. Dorfi and L.O'C. Drury, Simple adaptive grids for 1D initial value problems, *J. Comput. Phys.*, 69 (1987), pp.175-195.
[14] Q.Du and R. Nicolaides, Numerical studies of a continuum model of phase transition, *SIAM J. Numer. Anal.*, 28 (1991), pp.1310-1322.
[15] Q. Du, C. Liu and X. Wang, A phase field approach in the numerical study of the elastic bending energy for vesicle membranes, *J. Comput. Phys.*, 198 (2004), pp.450-468.
[16] Q. Du and J. Zhang, Adaptive finite element method for a phase field bending elasticity model of vesicle membrane deformations, *SIAM J. Sci. Comput.*, (2008), to appear.
[17] W.M. Feng, P. Yu, S.Y. Hu, Z.K. Liu, Q. Du, and L.Q. Chen, Spectral Implementation of an Adaptive Moving Mesh Method for Phase-field Equations, *J. Comput. Phys.*, 220 (2006), pp.498-510.
[18] H. Guillard, J.M. Mali and R. Peyret, Adaptive spectral methods with application to mixing layer computation, *J. Comput. Phys.*, 102 (1992), pp.114-127.
[19] S.Y. Hu and L.Q. Chen, A phase-field model for evolving microstructures with strong elastic inhomogeneity, *Acta Mater.*, 49 (2001), pp.1879-1890.
[20] W. Huang. Practical Aspects of Fourmulation and Solution of Moving Mesh Partial Differential Equations, *J. Comput. Phys.*, 171 (2001), pp.753-775.
[21] W. Huang and R.D. Russell, Moving mesh strategy based upon a gradient flow equation for two dimensional problems, *SIAM J. Sci. Comput.*, 20 (1999), pp.998-1015.
[22] W. Huang, Y. Ren and R.D. Russell, Moving mesh methods based on moving mesh partial differential equations, *J. Comput. Phys.*, 113 (1994), pp.279-290.
[23] W.C. Johnson and J.W. Cahn, Elastically induced shape bifurcations of inclusions, *Acta Metall.*, 32 (1984), pp.1925-1933.
[24] J. K. Lee, A study on coherency strain and precipitate morphology via a discrete atom method, *Met. Trans.*, 27A (1996), pp.1449-1460.
[25] R. Li, T. Tang, and P.-W. Zhang, Moving mesh methods in multiple dimensions based on harmonic maps, *J. Comput. Phys.*, 170 (2001), pp.562–588.
[26] J. Mackenzie, M.L. Robertson, A moving mesh method for the solution of the one-dimensional phase-field equations, *J. Comput. Phys.*, 181 (2002), pp.526-544.
[27] C. Mavriplis, Adaptive mesh strategies for the spectral element method, *Comput. Method. Appl. Mech. Eng.*, 116 (1994), pp.77-86.
[28] L. Mulholland, W. Huang, and D. M. Sloan, Pseudospectral solution of near-singular problems using numerical coordinate transformations based on adaptivity, *SIAM J. Sci. Comput.*,

19 (1998), pp.1261-1289.
[29] R. Mueller and D. Gross, 3D inhomogeneous, misfitting second phase particles-equilibrium shapes and morphological development, *Comput. Mater. Sci.*, 16 (1999), pp.53-60.
[30] K. Nakahashi, G.S. Deiwert, Three dimensional adaptive grid method, *AIAA J.* 24 (1986), pp.948-954.
[31] L.R. Petzold, Observations on an adaptive moving grid method for one-dimensional systems for partial differential equations, *Appl. Numer. Math.*, 3 (1987), pp.347-360.
[32] N. Provatas1, N. Goldenfeld and J. Dantzig, Efficient computation of dendritic microstructures using adaptive mesh refinement, *Phys. Rev. Lett.*, 80 (1998), pp.3308-3311.
[33] R. Sankarasubramanian, C. Jog and T. Abinandanan, Symmetry-breaking transitions in equilibrium shapes of coherent precipitates: Effect of elastic anisotropy and inhomogeneity. *Metallurgical and Materials Transactions*, 33 (2002), pp.1083-1090.
[34] S. Socrate and D. M. Parks, Numerical determination of the elastic driving force for directional coarsening in Ni-superalloys, *Acta Metall. Mater.*, 41 (1993), pp.2185-2209.
[35] X. Wang and Q. Du, Modelling and Simulations of Multi-component Lipid Membranes and Open Membranes via Diffuse Interface Approaches, *J. Math. Bio.*, 56 (2008), pp.347-371.
[36] Y. Z. Wang, L. Q. Chen, A. G. Khachaturyan, Three-dimensional dynamic calculation of the equilibrium shape of a coherent tetragonal precipitate in Mg-partially stabilized cubic ZrO2, *J. Amer. Ceramic Soc.*, 79 (1996), pp.987-991.
[37] A. Winslow, Numerical solution of the quasi-linear Poisson equation in a non-uniform triangle mesh, *J. Comput. Phys.*, 1 (1967), pp.149-172.
[38] D. Wang and X. Wang, A three-dimensional adaptive method based on the iterative grid redistribution, *J. Comput. Phys.*, 199 (2004), pp.423-436.
[39] S.M. Wise, J.S. Lowengrub, J.S. Kim and W.C. Johnson, Efficient phase-field simulation of quantum dot formation in a strained heteroepitaxial film, *Superlattices and Microstructures*, 36 (2004), pp.293-304.
[40] P. Yu, L. Chen and Q. Du, Applications of Moving Mesh Methods to the Fourier Spectral Approximations of Phase-Field Equations, in *Recent Advances in Computational Sciences: Selected Papers from the International Workshop on Computational Sciences and Its Education*, edited by Jorgensen et. al., World Scientific, 2007.
[41] P. Yu and Q. Du, A variational construction of anistropic mobility in phase-field simulation, *Discrete and Continous Dynamic Systems - B*, 6 (2006), pp.391-406.
[42] P. Yu, S. Hu, Q. Du and L.-Q. Chen. An iterative-perturbation scheme for treating inhomogeneous elasticity in phase-field models, *J. Comput. Phys.*, 208 (2005), pp.34-50.
[43] L. Zhang, L.-Q. Chen and Q. Du, Morphology of critical nuclei in solid state phase transformations, *Phys. Rev. Lett.*, 98 (2007), pp.265703.